Published in final edited form as:
J Neurotrauma. 2009 August ; 26(8): . doi:10.1089/neu.2008-0728.

Impact speed does not determine severity of spinal cord injury in mice with fixed impact displacement

Joong Hee Kim[1], **Tsang-Wei Tu**[2], **Philip V. Bayly**[2,3,*], and **Sheng-Kwei Song**[1,*]

[1] Department of Radiology, Washington University, St. Louis, MO, USA

[2] Department of Mechanical and Aerospace Engineering, Washington University, St. Louis, MO, USA

[3] Department of Biomedical Engineering, Washington University, St. Louis, MO, USA

Abstract

The speed of three leading rodent SCI impacting devices: 0.1 m/s (Infinite Horizon), 0.2 m/s (Ohio State Univerity), and 0.4 m/s (New York University) were investigated using a custom-fabricated impactor to determine its effect on mouse spinal cord injury severity. The spared white matter was examined at 7 and 21 days post injury with in vivo diffusion tensor imaging (DTI) and postmortem histology respectively. The neurological outcome of the injured mice was longitudinally evaluated using the Basso Mouse Scale. In vivo DTI derived diffusion anisotropy maps provided excellent gray-white matter contrast enabling objective and noninvasive quantification of normal appearing white matter. In vivo DTI estimated spared white matter content correlated well with those determined using postmortem histology. No significant difference in BMS was observed among injury groups of various impact speeds. The present results suggest that injury severity can be reproduced using speeds from 0.1 – 0.4 m/s at the fixed impact displacement.

Keywords

Contusion SCI; Impact speed; BMS; Diffusion tensor imaging; Spared white matter

Introduction

The rodent model of contusion spinal cord injury (SCI) has been widely employed for preclinical studies and is considered an appropriate model of human SCI (Young, 2002). Contusion injury devices, driven by gravity or electromagnetic force, induce traumatic injury by rapid deformation of the spinal cord tissue. The contusion SCI model has been developed in rodents to mimic damages caused by vertebral dislocation or “burst” fracture. Producing consistent, controlled, and reproducible injury, essential for the successful application of an animal contusion SCI model, has been achieved by applying advanced technology (electronics, mechanics, computer software, etc) in the design of injury devices (Rasband, 1997–2005; Stokes, 1992). Accurate monitoring of the mechanical parameters of impact by appropriate sensors reduces errors and enhances reproducibility of the performance of the impacting device.

[*]Send correspondence to: Sheng-Kwei “Victor” Song, Ph.D., Campus Box 8227, Washington University School of Medicine, Room 2313, 4525 Scott Ave. St. Louis, MO 63110, USA, Phone: (314) 362-9988, Fax: (314) 362-0526, ssong@wustl.edu. Philip V. Bayly, PhD, Department of Mechanical and Aerospace Engineering, Campus Box 1185, Washington University, 1 Brookings Dr. St. Louis, MO 63130, Phone: (314) 935-6081, Fax: (314) 935-4014, pvb@wustl.edu.

The use of mice in SCI studies is common, in part because of the availability of transgenic and knock-out animals that provide valuable insight into the mechanism of pathogenesis and repair. Three major devices, Ohio State University (OSU) (Jakeman et al., 2000; Rasband, 1997–2005), Infinite Horizon (IH) (Scheff et al., 2003) and the New York University (NYU) (Gruner, 1992; Kuhn and Wrathall, 1998) devices have been commonly used to generate controlled contusion SCI in mice. All these devices provide measurements of biomechanical parameters, including force on the spinal cord, impact displacement, and velocity of the impact tip. To generate injuries with consistent severity, various approaches have been employed. The NYU device produces consistent injury severity by accurate control of the height of its impacting rod; this generates consistent impact speed, which, for targets of similar compliance, leads to consistent force and impact depth. The OSU device controls severity of injury by precisely regulating the impact displacement, the depth of the impact tip traveling from dura in the cord. The IH device achieves this goal by the real time measurement and control of the force exerted on the cord.

The difficulty of producing consistent SCI injuries is partly attributed to the lack of a consensus identifying a single impact device that fits various research needs. One of the most distinct differences among the three major devices is the impact speed (or velocity) achieved at impact: 0.1 m/s (IH), 0.2 m/s (OSU), and 0.4 m/s (NYU). Thus, the effect of the impact speed on the severity of the mouse SCI model should be investigated. Recently, a linear relationship between impact displacement and the force exerted on the spinal cord by the IH device has been reported (Ghasemlou et al., 2005). Motivated by these results, we evaluated the effect of impact speeds of 0.1, 0.2, and 0.4 m/s, with an accurately controlled displacement of 0.8 mm.

Various methods have been used to evaluate the severity of SCI. Although histology is the “gold standard” for evaluating animal SCI severity, its invasive nature prohibits its application for longitudinal observations. Scoring of the animal’s behavioral outcome is a relevant, non-invasive, and widely-used metric (Basso et al., 1995, 1996; Basso et al., 2006; Engesser-Cesar et al., 2005). But this method lacks morphological and pathophysiological information on contusion-injured cords. For a better insight into the underlying injury, magnetic resonance imaging (MRI) has been employed as a noninvasive method to examine contusion-injured rodent spinal cord both ex vivo (Nevo et al., 2001; Nishi et al., 2007; Schwartz et al., 2005a; Schwartz et al., 2005b; Schwartz and Hackney, 2003) and in vivo (Bonny et al., 2004; Deo et al., 2006; Mihai et al., 2008).

In the present study, we examined the relationship between impact speed and injury severity using a custom fabricated electromagnetically-driven impact device. The accuracy of impact displacement was examined on a phantom and the mouse cord. The various injury severity was generated by fixing the displacement at 0.8 mm with three speficified impact speeds (0.1, 0.2, and 0.4 m/s). The injury severity was evaluated by assessing the daily hind limb motor function using Basso mouse scale (BMS) (Basso et al., 2006) and the extent of residual white matter using both in vivo diffusion tensor imaging (DTI) at 7 days post injury (DPI) and the postmortem Luxol fast blue (LFB) at 21 DPI. The in vivo DTI (7 DPI) and LFB (21 DPI) determined residual white matter extent consistently reflected the BMS scores. The injury severity assessed by the extent of residual white matter or BMS scores was not different for the three tested impact speeds.

Materials and Methods

Electromagnetic Driven Impactor

The custom-built impactor is shown in Fig. 1. The force of impact is provided by an electromagnetic actuator (Fig. 1a – D, BEI-Kimco Model LA15-16-024A, CA, USA).

Current is provided to the actuator via a linear amplifier (Precision MicroDynamics BTA-28V-6A, not shown in Fig. 1a). The trajectory is controlled by a plastic flexure, which restricts motion in all directions except the desired impact direction (Fig. 1a – E). The impactor is mounted on a precision XYZ table (Fig. 1a – C, ThorLabs PT3A) to provide fine adjustments of < 100 μm for locating desired target displacement. The desired impact displacement (displacement of impactor tip: Fig. 1a – H) is preset by digital micrometer (Parker-Hannifin/Daedal Division: Starrett 02064104). The micrometer provides a hard mechanical stop to limit the displacement of the impactor tip. The actual displacement of the impactor tip is measured by a laser displacement transducer (MicroEpsilon LD-1605), which provides fast, accurate measurements of tissue deformation (specified bandwidth > 5000 Hz).

The impactor is driven from a laptop PC using a Matlab program incorporating the Data Acquisition Toolbox (The MathWorks, Inc., Natick, MA). An analog IO card (National Instruments DAQCard 6062-E), which is capable of acquiring from all channels at 10KHz and providing analog output commands at the same rate, provides the interface between the PC and the impactor. A command (bold line in Fig. 1b) from the PC specifies the current provided by the linear amplifier, which in turn controls the force delivered by the linear actuator. “Phantom” data are acquired with three preset displacements (0.3 mm, 0.6 mm, and 0.9 mm) in both upward and downward directions (Fig. 1b).

Impact Procedures

The basic impact procedure is summarized with a schematic illustration and the measured displacement at different speeds (Fig. 2). After laminectomy, the mouse spine was supported in a custom-designed holder (Fig. 1a – I) and placed on a stage (Fig. 1a – B). The impactor tip is placed on top of the exposed cord by adjustment of the XYZ table (Fig. 1a – C). To determine the touch point, a conductivity sensor was used (Brody et al., 2007), with microscopic validation (Phase I in Fig. 2). After finding the zero position, the desired impact displacement was set by a digital micrometer (Fig. 1a – F). Impact was initiated by a bipolar command voltage signal (bold solid line in Fig. 2), amplified to a proportional current to the linear actuator (Fig. 1a – D). The impactor tip was driven by the generated electromagnetic force. The bipolar command first moved the impactor tip upward (Phase II in Fig. 2) and then rapidly downward (phase III in Fig. 2). The downward movement of impactor tip was stopped at the desired impact displacement by the modified digital micrometer. (Fig. 1a – F). After ~20 ms, the impactor tip was withdrawn above the initial position to avoid secondary impact (Phase IV in Fig. 2). Both command voltage and impact displacement were set and acquired using a laptop computer through the analog IO card as in the phantom measurement.

Spinal Cord Injury with Various Impact Speeds

All surgical interventions and both pre- and post-surgical care were performed in accordance with the Public Health Service Policy on Humane Care and Use of Laboratory Animals, *Guide for the Care and Use of Laboratory Animals* (Institute of Laboratory Animal Resources, National Research Council, 1996), and with the approval of the Washington University Institutional Care and Use Committee.

Twenty four ten-week-old female C57BL/6 mice weighing 18 ~ 20 g (Harlan, Indianapolis, IN) were anesthetized with an isoflurane and oxygen mixture (5 % for induction and 1.5% for maintenance). After a dorsal laminectomy at the T8 and T9 vertebral level, mice received contusive spinal cord injuries. Six mice (sham) received anesthesia, laminectomy, and underwent all procedures, including contact to establish the reference position, but no impact. Three injury groups of mice underwent contusion injury at 0.1, 0.2, and 0.4 m/s with

0.8 mm impact displacement using 1.3 mm diameter rounded tip. After impact, the site was closed in layers with 4-0 Silk sutures followed by subcutaneous administration of Baytril (2.5mg/Kg) and lactated ringers (5 ml). Standard postoperative care including bladder expression was provided in accordance to the manual of Spinal Cord Injury Research Training Program published by the Spinal Trauma and Repair Laboratories in Ohio State University (http://medicine.osu.edu/sci/).

Hind Limb Motor Function Evaluation

All mice underwent hind limb motor function evaluation with the BMS scale (Basso et al., 2006). All procedures were performed following the manual of Spinal Cord Injury Research Training Program held at Spinal Trauma and Repair Laboratories in Ohio State University (http://medicine.osu.edu/sci/). Briefly, two raters blinded to the experimental conditions observed hind limb motor function of contusion injured mice from 1 to 21 DPI. The rating was done daily in first week. Mice were rated every other day during the second week followed by ratings every three days in the third week. The worse deficit score was taken if two rater's scores did not match. At each time point, BMS score were averaged for each study group.

Animal Preparation for in vivo DTI

At 7 DPI, mice were delivered to MR facility and immobilized with an isoflurane and oxygen mixture (1.5% for maintenance). Core body temperatures were maintained at 37°C with a circulating warm water pad. Inhaled isoflurane-oxygen mixture was delivered to mice through a custom-made nose cone. The respiratory exhaust line was connected to a pressure transducer to synchronize DTI data acquisition with the animal's respiratory rate (Kim et al., 2006). An MRI-compatible restraining device was utilized to stabilize the vertebral column as reported previously (Kim et al., 2006). An inductively-coupled surface coil covering T8 – T10 vertebral segments (15 mm × 8 mm) was used as the RF receiver. A 9-cm i.d. Helmholtz coil was employed as the RF transmitter. The entire preparation was placed in an Oxford Instruments 200/330 magnet (4.7 T, 33-cm clear bore) equipped with a 15-cm inner diameter, actively shielded Oxford gradient coil (18 G/cm, 200-μs rise time). The magnet, gradient coil, and Techron gradient power supply were interfaced with a Varian UNITY-INOVA console (PaloAlto, CA) controlled by a Sun Microsystems Blade 1500 workstation.

In vivo Diffusion Tensor Imaging

A conventional spin-echo imaging sequence was modified by adding Stejskal-Tanner diffusion weighting gradients (Stejskal, 1965). The spin echo time (TE = 38 ms), time between application of gradient pulses (Δ = 20 ms), and diffusion gradient on time (δ = 7 ms) were fixed throughout the experiment. The repetition time (TR ~ 1.2 s) was varied according to the period of the respiratory cycle (~ 270 ms). During every breath, three different image slices were collected. Images were obtained with diffusion sensitizing gradients applied in six orientations: (Gx,Gy,Gz) = (1,1,0), (1,0,1), (0,1,1), (−1,1,0]), (0,−1,1), and (1,0,−1). Two diffusion-sensitizing factors (*b* values) of 0 and 1.0 ms/μm^2 were used. Eight scans were averaged per k-space line. The field of view was 10 × 10 mm^2 with 1.0 mm slice thickness and the image data matrix for each slice was 128 (PE) × 256 (RO) (zero filled to 256 × 256).

Data Analyses

Diffusion tensors were estimated independently for each voxel from the diffusion-weighted images using a weighted linear least-squares method (Koay et al., 2006). The eigenvalue decomposition was then applied to each tensor, yielding a set of eigenvalues ($\lambda_1 \geq \lambda_2 \geq \lambda_3$) and eigenvectors for each voxel. Maps of diffusion indices including relative anisotropy

(RA) and apparent mean diffusivity (<D>) were generated by applying the following equations for each voxel:

$$<D>=(\lambda_1+\lambda_2+\lambda_3)/3 \quad [1]$$

$$\mathrm{RA}=\frac{\sqrt{(\lambda_1-<D>)^2+(\lambda_2-<D>)^2+(\lambda_3-<D>)^2}}{\sqrt{3}<D>} \quad [2]$$

The RA map was additionally color coded to include information regarding the primary diffusion direction (i.e., the direction of the principle eigenvector). Specifically, the colors blue, red, and green correspond to rostrocaudal, mediolateral, and superoinferior diffusion directions, respectively, with the brightness of the color maps weighted by the RA (Pajevic and Pierpaoli, 1999).

To quantify the diffusion parameters, a region-of-interest (ROI) analysis was conducted. In control cords, the manual segmentation of ventrolateral white matter (VLWM) and ventral gray matter (VGM) was performed based on RA maps and the non-diffusion weighted image (b = 0 ms/μm^2). At T9 of control cords (n = 6), the RA histogram of VGM and VLWM were generated from manually segmented ROI producing mean and standard deviation (SD) for each VGM and VLWM. based on the histogram of the distribution of the control VGM and VLWM, the normal appearing white matter in VLWM region was determined by employing a threshold of mean + 2 × standard deviation of RA in the control VGM.

Tissue Preparation and Histological Analysis

At the conclusion of longitudinal hind limb motor function examinations, all mice were perfusion fixed through the left cardiac ventricle under deep anesthesia with 4 % paraformaldehyde in phosphate buffered saline (PBS) at pH 7.4. Following fixation, the spine was harvested, left in fixative for 24 hr, and then decalcified. A 2 mm segment of spinal cord centered at T9 was cut with the vertebral column intact after decalcification. Spinal cord blocks were embedded in paraffin and cut on a sliding microtome at a thickness of 3μm. For the examination of myelin integrity, luxol fast blue (LFB) staining was conducted. Briefly, the sectioned tissue underwent deparaffinization and rehydration. After overnight immersion in LFB solution (56 °C), excess stain was rinsed off and differentiation was performed with lithium carbonate solution and ethyl alcohol. After the completion of differentiation, tissue was mounted for microscopic inspection. Spared residual white matter volume for control and injured cord was evaluated utilizing ImageJ v 1.37 (Rasband, 1997–2005).

Statistical Analysis

Repeated measures ANOVA was employed to assess the difference of animal's hind limb motor function using SAS version 9.1.3. (SAS Institute Inc., Cary, NC, USA) with Tukey as post hoc test. The statistical significance was accepted as $p < 0.05$. At each time point, the group averaged BMS scores of the three injury groups were compared. The longitudinal variance of BMS within each study group including control was tested. One-way ANOVA was employed to examine the difference of spared white matter volume determined by sub acute in vivo RA and end point LFB. The significance of difference between control and injury groups, and among the three injury groups was tested. The in vivo RA threshold segmented normal appearing residual white matter volume of the injured cord was normalized to the averaged normal appearing white matter volume of control cords (n = 6).

The spared residual white matter volume determined by LFB was normalized to those of the control.

Results

The measured impact displacement (displacement of impactor tip) in “phantom” experiments and in the mouse spinal cord is shown as a function of time in Figs. 1b and 2. In both phantom and cord experiments, the downward speed was greater than the upward (negative sign). The overshoot (~0.02 mm), occurred in the fast downward movement, was insignificant compared to the desired impact displacement, preset by digital micrometer at 0.3, 0.6, and 0.9 mm (Fig. 1b). From contusion injured cord, consistent displacement (0.8 mm) and the regulated speed (from 0.1, 0.2, and 0.4 m/s) were observed with same duration at the maximum displacement (Fig. 2). The overshoot and undershoot of the impact displacement on mouse cord is also negligible compared to desired displacement at the speed ranging from 0.1 to 0.4 m/s.

Longitudinal hind limb motor function was evaluated (Fig. 3). All mice recovered from initial surgery and spinal shock during first week after injury. The BMS score of all injury groups were significantly lower than that of the control longitudinally ($F_{3,36} = 698.3$, $p < 0.001$). After 7 DPI, the BMS score reached steady state showing no statistically significant difference from 7 to 21 DPI for all groups ($p > 0.3$). No statistically significant difference in steady state BMS score was observed among three injury groups of different impact speeds ($p > 0.4$).

The serial in vivo DTI maps of the control and contusion injured cord at 7 DPI were localized based on both sagittal and coronal scout images (Fig. 4a). Gray scale and color coded RA maps showed clear gray-white matter contrast (Fig. 4b) even at the epicenter of the injured cord (Fig. 4c). The coherent blue color of the white matter was consistent with the structure of the myelinated axons (Fig 4b). The epicenter was easily identified through the significantly decreased RA (Fig. 4c).

An objective evaluation of the injury severity based on the normal-appearing VLWM was performed using RA threshold (Fig. 5). This RA threshold (= 0.47) was applied to the epicenter of all injured cords at 7 DPI to determine the extent of the normal-appearing VLWM volume (Fig. 6a). The normal-appearing VLWM extent of contusion injured cord was normalized to the averaged normal VLWM volume of control cords (Fig. 6b). There was not a statistically significant difference in the spared VLWM among all injury groups ($F_{2,15} = 0.0399$, $p > 0.7$) where there was a significant reduction from control ($F_{3,20} = 126.82$, $p < 0.001$: Fig. 6b).

At the end of longitudinal evaluation of BMS scores (21 DPI), the residual white matter at epicenter was assessed with LFB (Fig. 7a). Residual white matter was quantified by normalizing to the averaged total white matter volume from the control mice. Similar to the MRI findings at 7 DPI, there was no statistically significant difference in the residual white matter contents, determined using histology, among all injury groups at 21 DPI ($F_{2,15} = 0.2690$, $p > 0.7$). However, there was a significant reduction in spared VLWM in the injury groups comparing with the control ($F_{3,20} = 159.85$, $p < 0.001$; Fig. 7b).

Discussion

In this study, we examined the relationship between impact speed and injury severity in a mouse model of contusion SCI. Using a custom-built device that was set to a fixed impact displacement (0.8 mm), impact speed was varied over a range covering the three major rodent SCI devices (IH: 0.1m/s, OSU: 0.2 m/s, and NYU: 0.4 m/s). Multiple outcome

measures (hind limb motor function assessed with BMS, normal-appearing white matter determined using in vivo DTI, and postmortem spared white matter estimated by LFB) were evaluated at various time points (longitudinal BMS, in vivo DTI at 7 DPI, and LFB at 21 DPI). The current findings show no statistically-significant correlation between impact speed or injury severity at this fixed displacement.

The ability to control and reproduce different injury severities is crucial to evaluate treatment efficacy, as well as of the underlying mechanisms, of the injury. In this study, we regulated displacement and velocity using a custom-fabricated impactor. The displacement and trajectory were controlled using a flexure-based design (Fig. 1A – E). The extent of overshoot was reduced with micrometer-control and a rigid mechanical stop specifying impact depth. Insignificant overshoots (~ 0.02 mm) were observed in this study at a speed up to 0.4 m/s (Fig. 2).

The hind limb motor function has been widely employed to assess the injury severity (Basso et al., 1995, 1996; Basso et al., 2006; Engesser-Cesar et al., 2005; Magnuson et al., 2005) and the efficacy of treatments in rodent models of SCI (Engesser-Cesar et al., 2005; Steward et al., 2008). The longitudinal BMS suggested no significant difference in the hind limb motor function among the three injury groups of different impact speed. Even though behavioral tests are reliable and widely employed, it lacks the crucial localization information of the injury. DTI is a noninvasive modality that can provide quantitative assessments of SCI progression in rodents (Deo et al., 2006; Kim et al., 2007; Loy et al., 2007).

In vivo DTI was performed in mice at 7 DPI, coinciding with the steady-state of hind limb motor function assessed with BMS (Fig. 3). The normal-appearing VLWM at the epicenter was quantified since the hind limb motor function after injury would be strongly affected by the degree of white matter preservation at the epicenter (Kuhn and Wrathall, 1998; Ma et al., 2001; Nishi et al., 2007; Plemel et al., 2008). All injured cords had significantly reduced normal-appearing VLWM volume comparing with that of the control. However, all three injury groups showed similar normal-appearing VLWM volume at epicenter regardless of the impacting speed.

The spared white matter was also assessed with postmortem LFB at the conclusion of the course of the study. Similar to in vivo RA findings, the comparable extent of spared white matter was observed for all three injury groups. Even though RA and LFB were not measured concurrently, both measurements agreed in the location and extent of spared residual white matter.

In conclusion, the current finding suggests that speed variations spanning the range of three widely-employed rodent SCI impact devices (IH: 0.1 m/s, OSU: 0.2 m/s, and NYU: 0.4 m/s) do not affect injury severity if the displacement is controlled. In addition, estimates of spared white matter obtained using in vivo DTI derived RA maps compare closely with estimates from postmortem LFB, suggesting that in vivo DTI can be used to non-invasively measure white matter injury in the contusion injured spinal cord.

Acknowledgments

This study was supported in part by National Institute of Health NS047592, and the University of Missouri Spinal Cord Injuries Research Program. Authors thank Jian Wang for the insightful discussion and performing statistical analyses.

References

Basso DM, Beattie MS, Bresnahan JC. A sensitive and reliable locomotor rating scale for open field testing in rats. J Neurotrauma. 1995; 12:1–21. [PubMed: 7783230]

Basso DM, Beattie MS, Bresnahan JC. Graded histological and locomotor outcomes after spinal cord contusion using the NYU weight-drop device versus transection. Exp Neurol. 1996; 139:244–256. [PubMed: 8654527]

Basso DM, Fisher LC, Anderson AJ, Jakeman LB, McTigue DM, Popovich PG. Basso Mouse Scale for locomotion detects differences in recovery after spinal cord injury in five common mouse strains. J Neurotrauma. 2006; 23:635–659. [PubMed: 16689667]

Bonny JM, Gaviria M, Donnat JP, Jean B, Privat A, Renou JP. Nuclear magnetic resonance microimaging of mouse spinal cord in vivo. Neurobiol Dis. 2004; 15:474–482. [PubMed: 15056454]

Brody DL, Mac Donald C, Kessens CC, Yuede C, Parsadanian M, Spinner M, Kim E, Schwetye KE, Holtzman DM, Bayly PV. Electromagnetic controlled cortical impact device for precise, graded experimental traumatic brain injury. J Neurotrauma. 2007; 24:657–673. [PubMed: 17439349]

Deo AA, Grill RJ, Hasan KM, Narayana PA. In vivo serial diffusion tensor imaging of experimental spinal cord injury. J Neurosci Res. 2006; 83:801–810. [PubMed: 16456864]

Engesser-Cesar C, Anderson AJ, Basso DM, Edgerton VR, Cotman CW. Voluntary wheel running improves recovery from a moderate spinal cord injury. J Neurotrauma. 2005; 22:157–171. [PubMed: 15665610]

Ghasemlou N, Kerr BJ, David S. Tissue displacement and impact force are important contributors to outcome after spinal cord contusion injury. Exp Neurol. 2005; 196:9–17. [PubMed: 16023101]

Gruner JA. A monitored contusion model of spinal cord injury in the rat. J Neurotrauma. 1992; 9:123–126. discussion 126–128. [PubMed: 1404425]

Jakeman LB, Guan Z, Wei P, Ponnappan R, Dzwonczyk R, Popovich PG, Stokes BT. Traumatic spinal cord injury produced by controlled contusion in mouse. J Neurotrauma. 2000; 17:299–319. [PubMed: 10776914]

Kim JH, Budde MD, Liang HF, Klein RS, Russell JH, Cross AH, Song SK. Detecting axon damage in spinal cord from a mouse model of multiple sclerosis. Neurobiol Dis. 2006; 21:626–632. [PubMed: 16298135]

Kim JH, Loy DN, Liang HF, Trinkaus K, Schmidt RE, Song SK. Noninvasive diffusion tensor imaging of evolving white matter pathology in a mouse model of acute spinal cord injury. Magn Reson Med. 2007; 58:253–260. [PubMed: 17654597]

Koay CG, Chang LC, Carew JD, Pierpaoli C, Basser PJ. A unifying theoretical and algorithmic framework for least squares methods of estimation in diffusion tensor imaging. J Magn Reson. 2006; 182:115–125. [PubMed: 16828568]

Kuhn PL, Wrathall JR. A mouse model of graded contusive spinal cord injury. J Neurotrauma. 1998; 15:125–140. [PubMed: 9512088]

Loy DN, Kim JH, Xie M, Schmidt RE, Trinkaus K, Song SK. Diffusion tensor imaging predicts hyperacute spinal cord injury severity. J Neurotrauma. 2007; 24:979–990. [PubMed: 17600514]

Ma M, Basso DM, Walters P, Stokes BT, Jakeman LB. Behavioral and histological outcomes following graded spinal cord contusion injury in the C57Bl/6 mouse. Exp Neurol. 2001; 169:239–254. [PubMed: 11358439]

Magnuson DS, Lovett R, Coffee C, Gray R, Han Y, Zhang YP, Burke DA. Functional consequences of lumbar spinal cord contusion injuries in the adult rat. J Neurotrauma. 2005; 22:529–543. [PubMed: 15892599]

Mihai G, Nout YS, Tovar CA, Miller BA, Schmalbrock P, Bresnahan JC, Beattie MS. Longitudinal comparison of two severities of unilateral cervical spinal cord injury using magnetic resonance imaging in rats. J Neurotrauma. 2008; 25:1–18. [PubMed: 18355154]

Nevo U, Hauben E, Yoles E, Agranov E, Akselrod S, Schwartz M, Neeman M. Diffusion anisotropy MRI for quantitative assessment of recovery in injured rat spinal cord. Magn Reson Med. 2001; 45:1–9. [PubMed: 11146478]

Nishi RA, Liu H, Chu Y, Hamamura M, Su MY, Nalcioglu O, Anderson AJ. Behavioral, histological, and ex vivo magnetic resonance imaging assessment of graded contusion spinal cord injury in mice. J Neurotrauma. 2007; 24:674–689. [PubMed: 17439350]

Pajevic S, Pierpaoli C. Color schemes to represent the orientation of anisotropic tissues from diffusion tensor data: application to white matter fiber tract mapping in the human brain. Magn Reson Med. 1999; 42:526–540. [PubMed: 10467297]

Plemel JR, Duncan G, Chen KW, Shannon C, Park S, Sparling JS, Tetzlaff W. A graded forceps crush spinal cord injury model in mice. J Neurotrauma. 2008; 25:350–370. [PubMed: 18373484]

Rasband, WS. ImageJ. U.S. National Institutes of Health; Bethesda, MD: 1997–2005.

Scheff SW, Rabchevsky AG, Fugaccia I, Main JA, Lumpp JE Jr. Experimental modeling of spinal cord injury: characterization of a force-defined injury device. J Neurotrauma. 2003; 20:179–193. [PubMed: 12675971]

Schwartz ED, Chin CL, Shumsky JS, Jawad AF, Brown BK, Wehrli S, Tessler A, Murray M, Hackney DB. Apparent diffusion coefficients in spinal cord transplants and surrounding white matter correlate with degree of axonal dieback after injury in rats. AJNR Am J Neuroradiol. 2005a; 26:7–18. [PubMed: 15661691]

Schwartz ED, Cooper ET, Fan Y, Jawad AF, Chin CL, Nissanov J, Hackney DB. MRI diffusion coefficients in spinal cord correlate with axon morphometry. Neuroreport. 2005b; 16:73–76. [PubMed: 15618894]

Schwartz ED, Hackney DB. Diffusion-weighted MRI and the evaluation of spinal cord axonal integrity following injury and treatment. Exp Neurol. 2003; 184:570–589. [PubMed: 14769351]

Stejskal E, Tanner JE. Spin Echoes in the Presence of a Time-Dependent Field Gradient. J Chem Phys. 1965; 42(1):288–292.

Steward O, Sharp K, Yee KM, Hofstadter M. A re-assessment of the effects of a Nogo-66 receptor antagonist on regenerative growth of axons and locomotor recovery after spinal cord injury in mice. Exp Neurol. 2008; 209:446–468. [PubMed: 18234196]

Stokes BT. Experimental spinal cord injury: a dynamic and verifiable injury device. J Neurotrauma. 1992; 9:129–131. discussion 131–124. [PubMed: 1404426]

Young W. Spinal cord contusion models. Prog Brain Res. 2002; 137:231–255. [PubMed: 12440371]

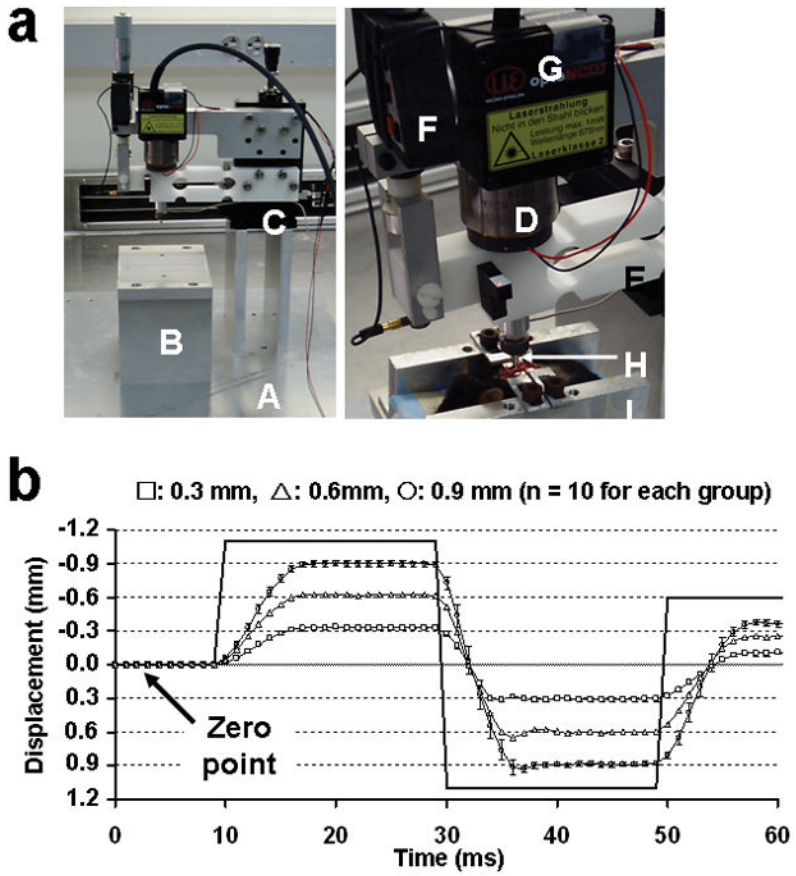

Figure 1.

The custom-built impact device (a): A – XY plate, B – stage for mouse, C -XYZ translator, D – linear actuator (provides electromagnetic force), E – flexure (restricts motion so impactor tip moves only at the desired z-direction), F – digital micrometer (used to set the impact distance), G - laser displacement transducer (measures the impact distance, i.e., displacement of the impactor tip), H – impactor tip (13 mm diameter), I – mouse holder; (b) measured impact displacements during phantom impacts (n=10) at various impact depths: 0.3 mm (□), 0.6 mm (△), and 0.9 mm (○). Data is expressed as mean ± standard deviation. Since the impact is conducted from the dorsal to ventral direction, a negative sign represents upward motion. The solid, bold line represents the command pulse (voltage, not related to the y-axis units). The zero point is indicated with an arrow. These displacement profiles during phantom impacts show high correspondence with desired trajectories, at impact depths from 0.3 to 0.9 mm, for both upward and downward motion.

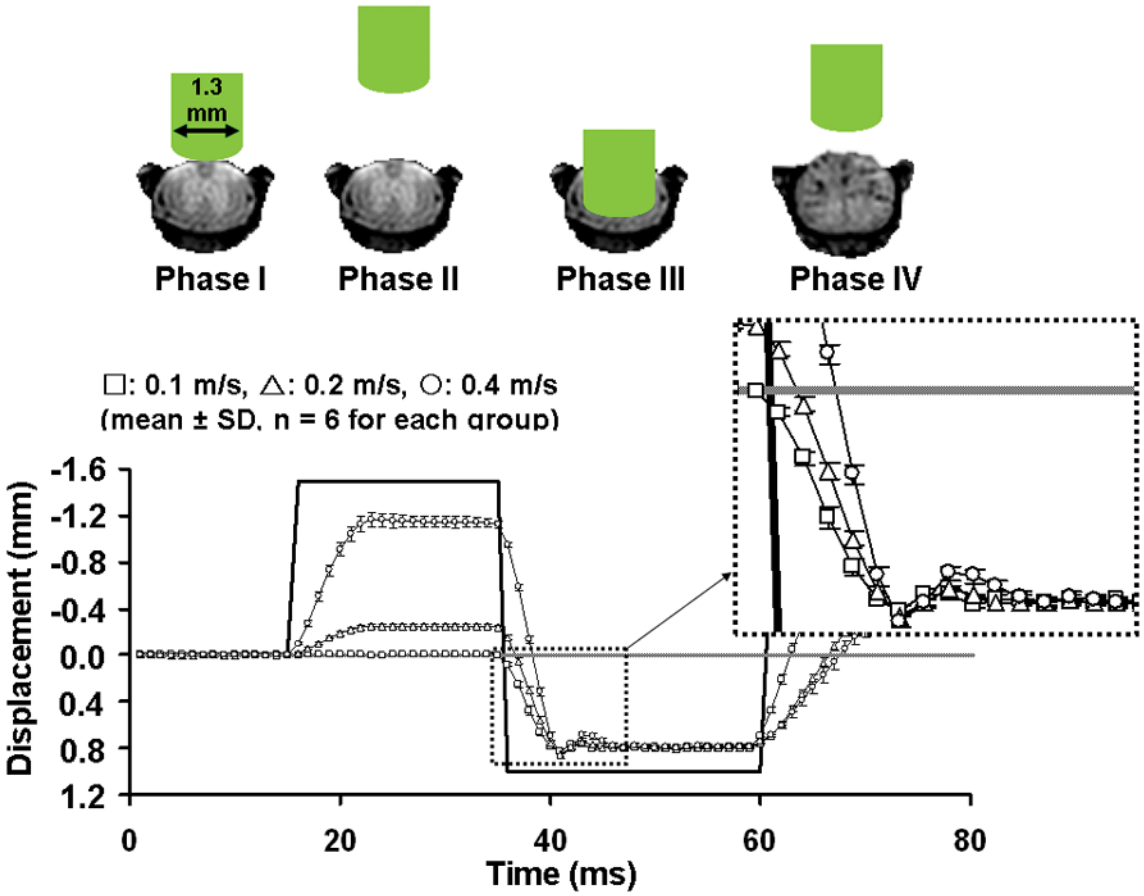

Figure 2.

The impact procedure on the mouse spinal cord is shown, along with a plot of the position of the impactor tip vs. time. The bold solid line represents the command pulse, in voltage (the amplitude is not to scale) and the displacement for 0.1 m/s (□), 0.2 m/s (△), and 0.4 m/s (○) are presented as mean ± standard deviation (n = 6 for each group). Negative displacements represent the upward motion (from ventral to dorsal). Prior to phase I, the impactor tip was placed directly on top of the exposed cord by the XYZ translator. With the initiation of impact procedure via a computer command, the impactor tip was moved up (phase II) and rapidly down (impact occurs, phase III). The impactor tip was immediately moved up to avoid secondary impact.

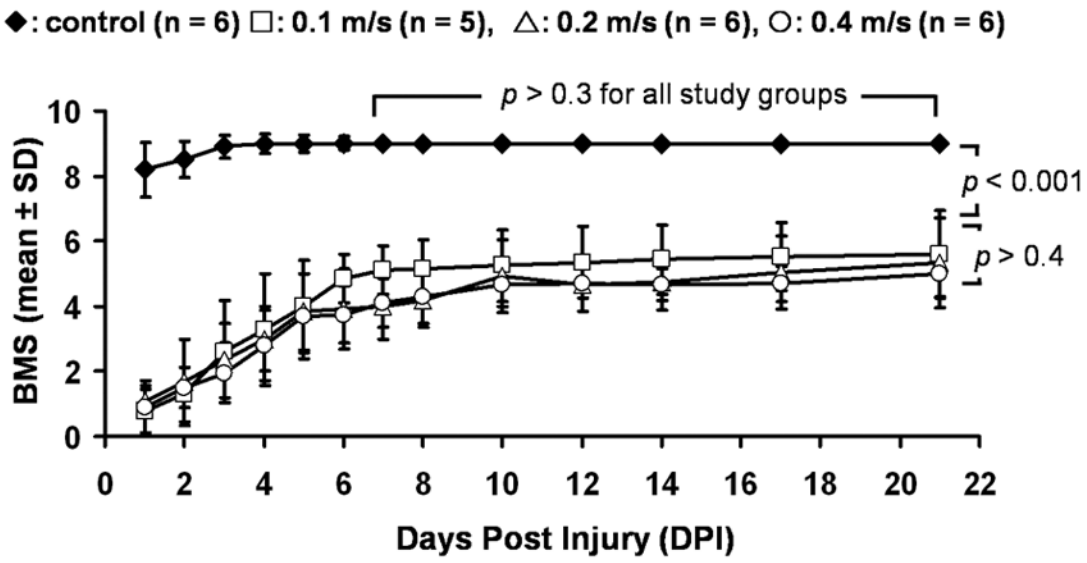

Figure 3.

Longitudinal Basso mouse scale (BMS) for control (◆), and impacts at 0.1 m/s (□), 0.2 m/s (△), and 0.4 m/s (○). Results are presented as mean ± standard deviation. All groups recovered from the initial severe functional deficit reaching a steady state BMS score (5 ± 0.8) after 7 DPI. No significant functional differences among injury groups were observed where all injury groups have significantly lower score than the control.

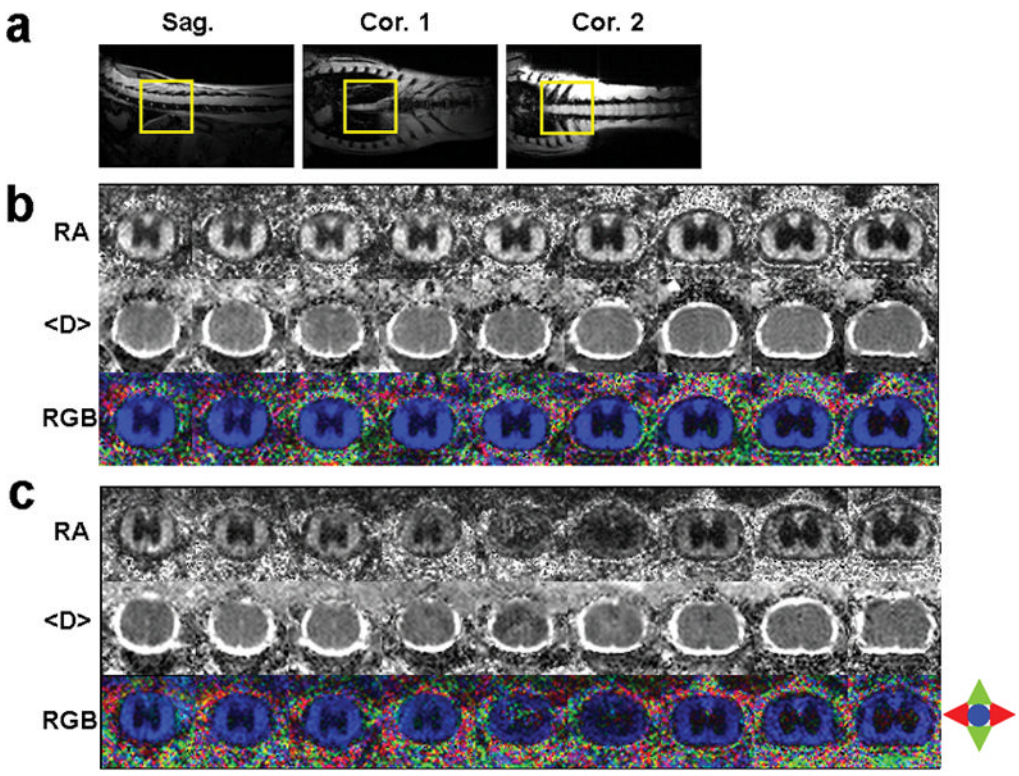

Figure 4.

(a) Scout sagittal and coronal images, (b) serial transverse in vivo diffusion tensor images of the control, and (c) injured cords are demonstrated. Nine contiguous transverse (or axial) images were acquired encompassing T7 – T10 vertebrae level (voxel size = 39 μm × 39 μm (zero-filled); slice thickness =1 mm). Relative anisotropy (RA) and apparent mean diffusivity (<D>) are displayed in scale of 0 – 1.414 and 0 – 2 μm^2/ms. The parenchyma of the spinal cord is hypointense compared to the surrounding bright CSF in the <D> map. The gray-white matter contrast is clearly seen in the RA map. The coherent directionality of white matter is obvious in the color coded RA map where red is left to right, green is up and down, and blue is in and out of the image plane. The epicenter of the injury is easily identified from the RA map.

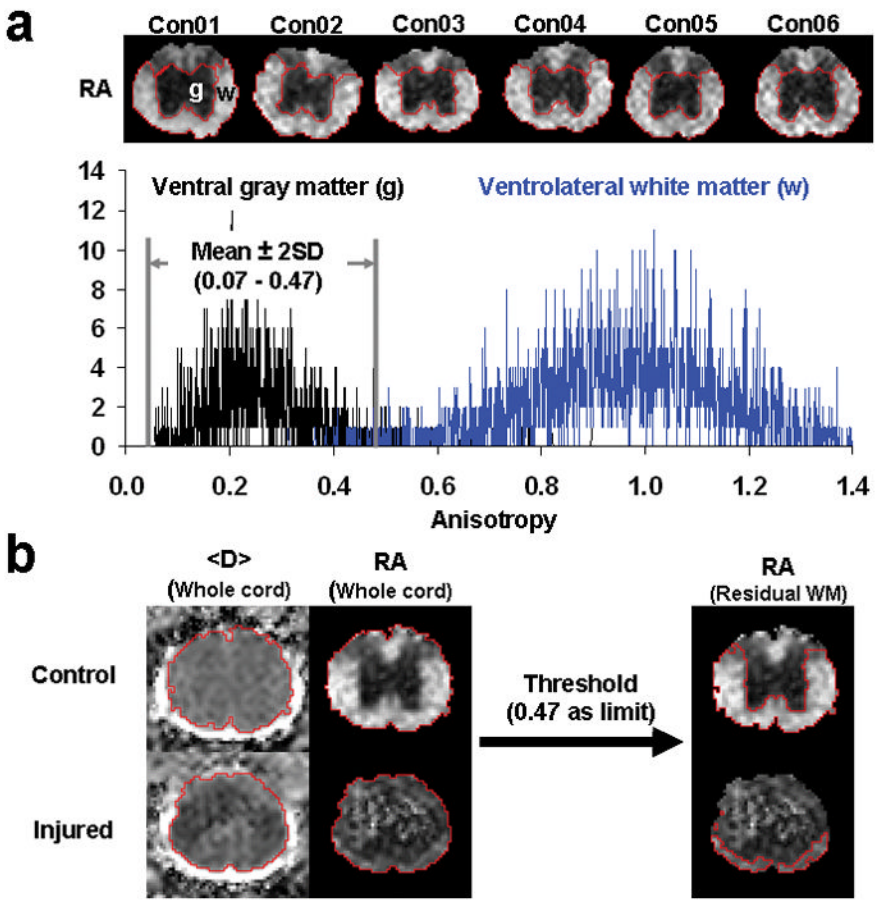

Figure 5.

The anisotropy distribution of ventral gray matter (VGM, g) and ventrolateral white matter (VLWM, w) from 6 control mice (Con01 – Con06) are shown with dorsal gray and white matter excluded (a). Two normally distributed RA values are clearly seen from VGM (0.27 ± 0.10) and VLWM (0.97 ± 0.19). All data are presented as mean ± standard deviation. A threshold of RA = mean + 2 × standard deviation, i.e., 0.47, of VGM was employed to successfully separate the ventrolateral white matter from the gray matter (b).

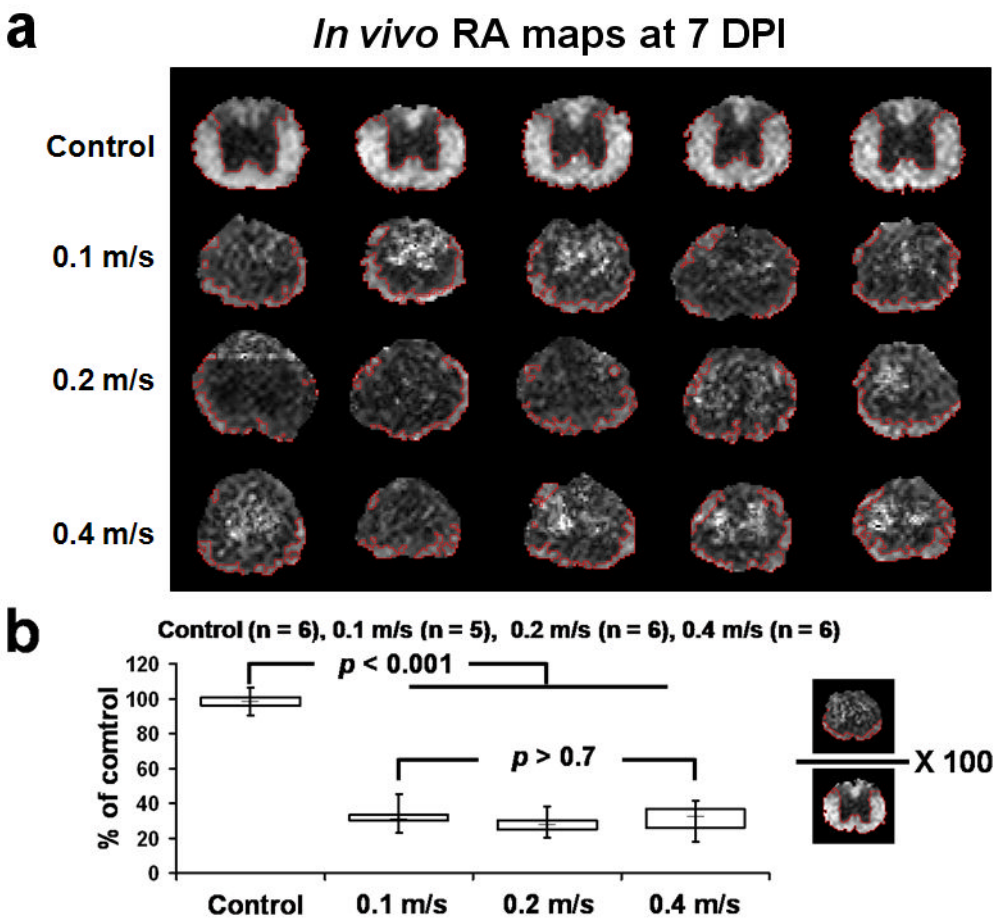

Figure 6.

The normal-appearing residual VLWM determined using the RA threshold (Fig. 5) at the epicenter from 5 individual mice is displayed (a). Control cords have ROIs containing entire ventrolateral white matter. All injured cords show normal appearing residual white matter mostly at the outer rim of the parenchyma. The normal-appearing VLWM volume, normalized to the control, for control (n = 6), 0.1 m/s (n = 5), 0.2 m/s (n = 6), and 0.4 m/s (n = 6) groups at 7 DPI were obtained. All injured groups show a significant decrease in the normal-appearing VLWM volume compared with that of the control. There is no statistically significant difference among all injured groups.

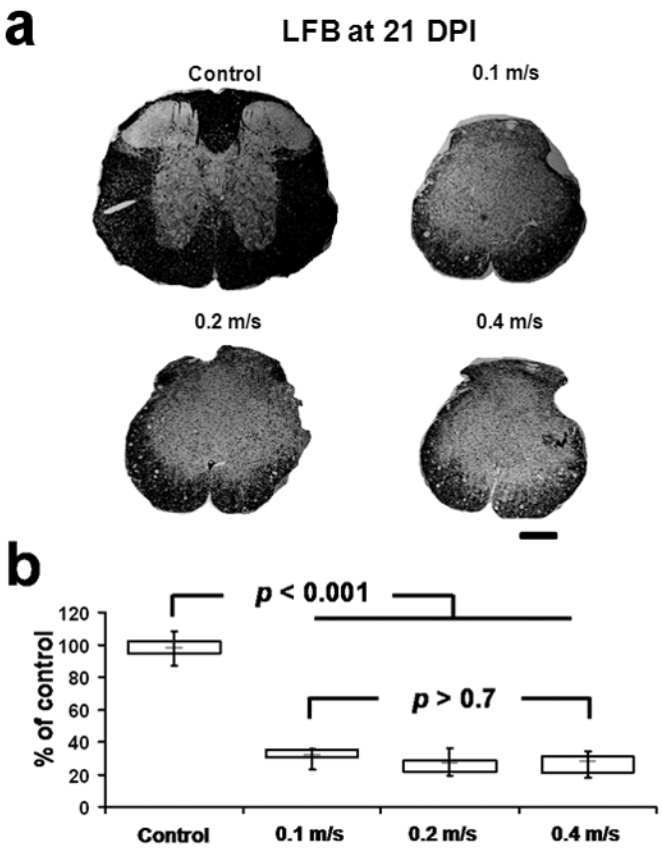

Figure 7.
Luxol fast blue (LFB) staining at the epicenter of injury (a), and the residual VLWM volume at 21 DPI for control (n = 6), and injury groups of impact speed at 0.1 m/s (n = 5), 0.2 m/s (n = 6), and 0.4 m/s (n = 6) (b). The scale bar represents 100 μm. The spared residual white matter volume of the injured cord is normalized by the averaged volume of control cords. The residual white matter of the injured cords is significantly smaller than the control, but there is no statistically significant difference among injured cords.